Transcriptional changes are regulated by metabolic pathway dynamics but decoupled from protein levels

Feltham, J[1]., S. Xi*[1], S. Murray*[1], M. Wouters[1], J. Urdiain-Arraiza[1], C. George[1], A. Townley[1], E. Roberts[1], R. Fisher[2], S. Liberatori[1], S. Mohammed[1], B. Kessler[2] and J. Mellor[1]

1 Department of Biochemistry, University of Oxford, South Parks Road, Oxford, OX1 3QU.

2 Nuffield Department of Medicine, University of Oxford, Henry Wellcome Building for Molecular Physiology, Old Road Campus, Headington, Oxford, OX3 7BN

Contact: jane.mellor@bioch.ox.ac.uk

*Equal contribution

Summary

The central dogma of molecular biology states that information flows from DNA to protein via RNA (Crick, 1970). This model is central to our understanding of biology but can lead to the assumption that changes in transcription and transcripts will inevitably lead to changes in protein levels, and so directly impact the metabolic and biosynthetic state of the cell. To test this assumption, we used a biological system characterised by genome-wide, cyclical changes in transcription, to assess whether changes in transcription are reflected in changes at the level of protein. We reveal that despite large changes in transcription at the majority of genes, there is little change in protein. This decoupling results from the slow rate of protein turnover. The changes protein activity we did observe were instead a reflection of the metabolic state of the cell, resulting from post-transcriptional modifications such as acetylation and phosphorylation, that in turn drive the cycling of processes such as transcription and ribosome biogenesis. Thus, transcriptional and transcript cycling reflects rather than drives the metabolic and biosynthetic changes during biological rhythms. We suggest that caution is needed when inferring the activity of biological processes from transcript data, as this reflects but does not predict a cell's state.

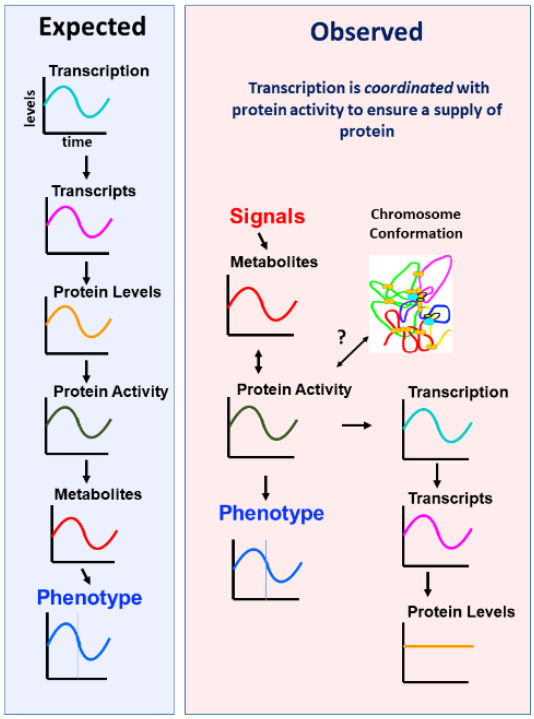

Introduction

The central axis of gene-expression, that RNA synthesis is ultimately required for protein synthesis, is clearly evident in eukaryotic cells and the relationship between RNA and protein is universally accepted. In response to developmental cues and stress-responses, transcriptional induction or RNA stabilization of protein-coding genes drives accumulation of their protein products. The proteins in turn remodel cellular physiology to respond to that stimulus (Banerji et al., 1984; Storti et al., 1980; Tissieres et al., 1974). The ubiquity of this underlying axis of information-transfer can easily draw one to the conclusion that whenever transcription changes, protein abundance will follow suit. However, recent studies have demonstrated that this assumption may not be correct (Caster et al., 2016; Liu et al., 2016; Noya et al., 2019; Ray and Reddy, 2016).

Cycling transcription is a universal feature of eukaryotic biological rhythms and the yeast metabolic cycle provides an ideal model for how changes in transcription affect the proteome (Causton et al., 2015; Klevecz et al., 2004; Kuang et al., 2014; Mellor, 2016; Tu et al., 2005; Tu and McKnight, 2006).

In this study we perform a multiomics analysis (Sanchez-Gaya et al., 2018) of the YMC, from the level of transcription through to the proteome. In the process, we reveal that protein turnover rates can completely attenuate cycling transcription and that transcriptional changes are often the consequence, rather than the cause, of changes in cellular physiology.

Results

To assess nascent transcription and transcript levels, 11 calibrated NET-Seq (Churchman and Weissman, 2011; Fischl et al., 2017) libraries were generated alongside 22 calibrated polyA-primed RNA-Seq libraries, throughout the synchronised biological rhythm of *S.cerevisiae*. Position in the rhythm was monitored using the change in dissolved O_2 in the growth medium (Figure S1A,B), partitioning cycling into phases of high and low oxygen consumption (HOC, LOC). When plotted over time total transcription rates remained largely constant, with a range of expression of 1.2-fold (Fig 1A). The NET-Seq libraries were log2 fold-change vs median (LFCM) transformed then divided into three clusters, as recommended by the gap-statistic, using the k-means++ algorithm (Figure 1B and Figure S1). When same transformation was applied to the RNA-Seq data, the close relationship between transcription and transcripts is clear (Figure 1C). Some discrepancies in the dynamics of transcription and transcript levels were observable in Figure 1C, suggesting differential transcript stability and were investigated by subclustering the HOC-T, LOC-T and TI-T clusters using the RNASeq data. Gap-Statistic analysis revealed that LOC-T and TI-T did not require further clustering, but HOC-T could be divided into three subclusters, each of which exhibited distinct RNASeq profiles.

The transformed data was plotted over time (Figure 1D). The non-cycling cluster (TI-T, 3926/5579 of genes), resembled total transcription (mean NET-Seq range 1.3-fold). The two smaller clusters showed markedly distinct profiles, with large log2 fold-changes that coincided with the HOC phase of the rhythm. One cluster exhibited an antiphase oscillation with maximum transcription and transcript levels during the LOC phase (cluster LOC-T, 805 genes, mean NET-Seq range 2.7-fold, mean RNA-Seq range 4.2-fold). The second cluster containing 848 genes, peaked in expression during the HOC phase (cluster HOC-T, mean NET-Seq range 6.5-fold, mean RNA-Seq range 10.8-fold), before dropping sharply at the HOC/LOC boundary then returning to basal expression levels and was enriched for ribosomal protein genes (RPGs) and ribosome biogenesis genes (RiBi) (Figure S1). The peaks in transcripts encoding components of the ribosome, or enzymes of metabolic pathways (Fig. S2 GOs for other clusters), is widely assumed to reflect peaks in protein levels which in turn *cause* the changes in metabolic state that characterize this rhythm (Kuang et al., 2014; Tu et al., 2005; Tu and McKnight, 2006).

To address this directly, we generated two proteomes from synchronized wild-type cells, one with and one without TMT-labelling. We observed a strong overlap in the representation of the proteome in the two datasets and strong representation of all three mRNA clusters (Figure 2A & B). The TMT-labelled proteome, along with its corresponding transcriptome data, was plotted as LFCM for each mRNA cluster (Figure 2C). Despite the cluster members showing their characteristic profiles at the RNA level, their protein levels remained constant over time (mean protein range <1.15-fold). This is also shown in the differences between the coefficients of variation (CoV) for mRNA levels and proteins levels of the HOC-R, LOC-R and TI-R clusters (Figure 2D). Furthermore, the autocorrelation of the mRNA was generally strongly positive for all clusters, demonstrating smooth and continuous changes in expression over time, whereas the coefficients for the proteomics data centre around zero, implying that the small changes in that occur in the proteomics data are largely the result of statistical noise (Figure 2E).

We considered three models to understand how the disconnect between the proteome and transcriptome arose (Figure 3A). Our data suggest that protein synthesis levels are low throughout the rhythm but cycle with transcripts. First, active protein synthesis was detected over most of the rhythm using the puromycin incorporation assay (Figure 3B). Additionally, calibrated RiboSeq (Ingolia et al., 2009) metagenes revealed that triplet periodic reads were present in RiboSeq libraries from synchronized cells, albeit at far lower levels than in log-phase (Figure 3C). Consistently, ribosome occupancy assessed using polysome profiling was dramatically different from exponential growth, primarily monosomes (Figure 3D). Next by sequencing poly(A)-primed RNASeq libraries, prepared from the input and monosomal fractions of gradient-fractionated cell lysate, we show that translation of genes is a simple function of their transcript levels (Figure 3E & F). Therefore, the proteome must be buffered at the level of degradation, rather than translation, and this is likely to reflect slow-turnover as the median half-life of protein is around 17.2 hours (Lahtvee et al., 2017) and negatively correlate with the degree of variation in protein levels through the rhythm. This supports proteins being exceptionally stable under cycling conditions as the most likely explanation for the invariant proteome (Figure 3G).

Considering the possibility that lowly transcribed genes would be differently amenable to changes in transcription levels to highly transcribed ones, we plotted the absolute log2-NETSeq signals by cluster (Figure 1D). Surprisingly, all clusters showed similar variation in expression and, although HOC-T and LOC-T both cycled over several orders of magnitude, substantial levels of transcription were observed even at the lowest points. Additionally, this remained the case regardless of the median level of transcription (Figure 1E).

Rps6 phosphorylation is a well-studied target of the nutrient-sensing TOR-signalling pathway and a marker of ribosome biogenesis (Gonzalez et al., 2015; Yerlikaya et al., 2016). In order to determine whether the levels of phospho-Rps6p, and by extension 40S-subunit assembly, vary during the rhythm, we probed western blots for phospho-Rps6p (Figure 4A). Phospho-Rps6p showed a significant enrichment in HOC-phase versus LOC-phase, increasing in abundance by several orders of magnitude which suggests that TOR-signalling and 40S assembly vary across the YMC, peaking in HOC-phase. Indeed, in line with Rps6p phosphorylation, rRNA transcription rates were low during LOC-phase and peaked during HOC supporting cycling TOR signalling coordinating ribosome biogenesis across this rhythm (Figure 4B). Intriguingly, ribosomal protein (RP) levels were constant over time which we interpret as implying the existence of an excess pool of chaperone-bound RPs that are drawn-upon to assemble ribosomes during HOC-phase (Figure S1B).

Histone acetylation is known to vary over biological rhythms and acetylation of the histones at the promoters of genes is associated with active transcription and binding of chromatin remodelling

complexes (CRCs) (Kuang *et al.,* 2014, Cai *et al.,* 2011, circadian rhythm and transcription references) . Plotting the NET-Seq data alongside acetly-H3 ChIP-Seq data for the HOC-T and LOC-T genes reveals that the changes in expression that they exhibit during HOC-phase follow changes in histone acetylation status at the same promoters (Figure 4C). Interestingly, changes in the transcription of these genes are also associated with binding of the RSC-complex component Rsc2p (Cairns et al., 1996; Jambunathan et al., 2005) to their gene bodies (Figure 4D). Thus, we propose that the changes in transcription of HOC-T and LOC-T promoters through the YMC are driven by a shift in acetylation from one class of promoters to the other titrating limiting PIC components and CRCs between promoter classes.

Discussion

The assumption that transcription/translation feedback-loops control and define the phases of the biological rhythms that underlie all cells is false. Instead, biological rhythms appear to be regulated through changes in metabolism and the activity of signalling complexes such as TOR, PKA, SAGA, CK1, GSK3 and Tip60 (Cai and Tu, 2011; Causton et al., 2015; Lee and Tu, 2015). Indeed, regulation of protein activity through metabolites and post-translational modifications makes for a much more economical way of regulating biological rhythms than bulk remodelling of the cellular proteome.

By demonstrating complete decoupling of transcript and protein levels, we highlight how using the transcriptome as a proxy for gene expression can result in misleading conclusions. Thus, when considering the impact of an internal or external perturbation of gene expression on cellular phenotype, it is critical to measure the effect that it has on protein levels. Additionally, our findings highlight the underappreciated importance of protein stability in controlling gene-expression dynamics, as it is at this stage of gene-expression where we propose that cycling transcription is silenced.

A major question that emerges from this work is "if the proteome remains unaffected, what is the function of transcriptional cycling across biological rhythms?". One intriguing possibility is that transcription may have additional roles in cellular physiology, aside from RNA synthesis. Transcription and the chromatin environment are deeply intertwined and extensively remodel one another (Kouzarides, 2007; Skalska et al., 2017). Furthermore, both processes are directly controlled by metabolism as certain core metabolic enzymes such as Hxk2p, and kinases such as TOR, can bind to the DNA via transcription factors and regulate promoter activity (Ahuatzi et al., 2007; Herrero et al., 1998; Tsang et al., 2010; Vega et al., 2016). Perhaps the role of transcription in biological rhythms is to coordinate and regulate signalling pathways by converting the chromatin into a platform upon which signalling complexes can form and interact with one another?

Alternatively, it is possible to simply dismiss the cycling transcriptome as a spandrel; a process that occurs not because of any inherent adaptive advantage but because it is a relatively harmless consequence of other beneficial properties of cellular physiology. It is crucial for the cellular transcriptional machinery to be responsive to external nutrient signals such as changes in carbon and nitrogen availability in order to allow the cell to adapt to changes in its environment. Accordingly, it is possible that this nutrient-sensitivity is also enough to drive changes in transcription as a result of the changing intracellular metabolite levels that occur during biological oscillations. This hypersensitivity, if present, would not be selected against due to its lack of effect on the proteome. As such, it might be allowed to persist to ensure that cells are able to sense and respond to changes when this is required of them?

In summary, we find that the eukaryotic proteome is able to buffer changes in transcript abundances through slow protein-turnover, highlighting the importance of direct measurements of the proteome

when making inferences about phenotype. Furthermore, cycling of transcription in the absence of cycling proteins implies that additional functions for transcription may exist aside from gene-expression.

References

Lead Contact and Materials Availability

As Lead Contact, Jane Mellor is responsible for all reagent and resource requests. Please contact Jane Mellor at jane.mellor@bioch.ox.ac.uk with requests and inquiries.

Method Details

Genetic manipulation of yeast strains

All strains used in this study are listed in the KEY RESOURCES TABLE. Genetic manipulation of strains was carried out using the homologous recombination method described by (Longtine et al., 1998). For gene deletion strains, PCR products were made containing a selection marker with promoter and terminator sequences flanked at both ends by 40bp of sequence homologous to sequences either side of the region to be deleted. For 3xFLAG tagged strains, first a plasmid was created from plasmid pFA6a-GFP(S65T)-His3MX6 (Longtine et al., 1998) with the 3xFLAG sequence amplified from strain YSC001 by PCR inserted in place of GFP. PCR products were made using this template consisting of a 40bp sequence homologous to the first 40bp upstream of the stop codon of the gene to be tagged followed by the FLAG sequence, His5 selection marker and 40bp of sequence homologous to a region downstream of the gene to be tagged. 3xHA tagged strains were created in a similar manner using the pFA6a-3HA-KanMX6 plasmid (Longtine et al., 1998).

Cells to be transformed were grown to log phase, pelleted, re-suspended in 450 µL 0.1 M LiAc/TE and incubated (> 1 hr, 4°C). 100 µL of cell suspension, 10 µL of gel-extracted PCR product, 10 µL calf thymus DNA (Sigma D8661), 700 µL 0.1 M LiAc/TE, 40% PEG were incubated (30 min, 30°C) then heat-shocked (20 min, 42°C). Cells were pelleted (5 min, 7000 rpm), re-suspended in H_20 and plated onto appropriate selection media. DNA was extracted from transformants, screened by PCR and confirmed by sequencing.

Metabolic Cycles

Fermentors were Bioflo320 (2 l vessel, 1.1 l culture volume – New Brunswick) or Minifor (400 ml vessel, 200 ml culture volume - Lambda) as indicated and cultures were grown in either YMC-YE media (pH 3.5 - ammonium sulphate 5 g/l, pottassium dihydrogen monophosphate 2 g/l, magnesium sulphate 0.5 g/l, calcium chloride 0.1 g/l, yeast extract 1 g/l (Difco), glucose 10 g/l, sulphuric acid 0.035 %, antifoam-204 0.05 % (Sigma-Aldrich), iron sulphate 20 mg/l, zinc sulphate 10 mg/l, manganese chloride 1 mg/l, copper sulphate 10 mg/l) or YMC-MD media (pH 3.5 - ammonium sulphate 5 g/l, pottassium dihydrogen monophosphate 2 g/l, magnesium sulphate 0.5 g/l, calcium chloride 0.1 g/l, glucose 2.5 g/l, sulphuric acid 0.0067 %, antifoam-204 0.05% (Sigma-Aldrich), iron sulphate 20 mg/l, zinc sulphate 10 mg/l, manganese chloride 1 mg/l, copper sulphate 10 mg/l, biotin 2 ug/l, calcium pantothenate 400 ug/l, folic acid 2 ug/l, inositol 2 mg/l, niacin 400 ug/l, p-aminobenzoic acid 200 ug/l, pyridoxine HCl 400 ug/l, riboflavin 200 ug/l, thiamine HCl 400 ug/l) as indicated. Fermenter runs were initiated with the inoculation of 10 ml starter culture that had been grown overnight to saturation at 30°C. BioFlo320 runs were operated at aeration rates on 1-5 l/min and agitation rates of 600-1000

rpm whilst Minifor runs were operated at an aeration rate of 0.15 l/min and agitation rate of 3.0 Hz. All runs were operated at 30°C and maintained at pH 3.5 through the addition of 0.25 M NaOH. Cells were grown to saturation (OD_{600} 16.0: YMC-YE; OD_{600} 4.0: YMC-MD) and starved for a minimum of 6 hours. Following starvation, continuous culture was maintained through the infusion of fresh media at a dilution rate of 0.082 hr^{-1}.

NET-seq/Riboseq

Yeast culture

For NET-seq, 100 ml of cycling *CENPK113-7D rpb3-FLAG* was harvested by filtration onto a 0.45 µm pore size, 90 mm diameter nitrocellulose filter paper (Whatman). Cells were scraped off the filter paper with a spatula pre-cooled in liquid nitrogen and flash frozen in liquid nitrogen. Flash-frozen *S. pombe* cells were added at a mass ratio of 1:5 and cells were ground in 6 cycles of 3 min at a 15 Hz shaking frequency in a 50 mL grinding jar (Retch) with a 25 mm stainless steel ball using a Retsch MM400 mixer mill. The grinding chamber was cooled in liquid nitrogen in between cycles. 1 g of yeast grindate was stored at −80°C. For RiboSeq, 50 ml of cycling *CENPK113-7D rpb3-FLAG* was harvested and ground as above, and 0.5 g of yeast grindate was stored at -80°C.

RNase-Protection and Monosome Isolation.

0.5 g of yeast grindate was resuspended in 2.5 ml RiboSeq lysis buffer (20 mM Tris HCl pH 8.0, 150 mM NaCl, 5 mM $MgCl_2$, 1% Triton-X100, 100 ug/ml cycloheximide, 1 mM DTT). 250 ul of lysate was digested with 7.5 ul RNaseI (Ambion) for 45 min on a nutator (25°C) and monosomes were isolated from the void volume of Illustra MicroSpin S-400 columns (GE Healthcare). Small RNAs were extracted using the miRNeasy kit (Qiagen) and RNA fragments of 26-35 nts in length were isolated using TBU-PAGE (see size-selection).

Immunoprecipitation (IP - NET-seq)

1 g of yeast grindate was resuspended in Lysis buffer A (20 mM HEPES (pH 7.4), 110 mM KOAc, 0.5% Triton X-100, 0.1% Tween 20, 10 mM $MnCl_2$, 1x proteinase inhibitors (complete, EDTA-free (Roche)), 50 U/ml SUPERase.In (Invitrogen)). Resuspended grindate was incubated (4°C, 20 min) with 660 U of DNase I (Promega). Insoluble cell debris was pelleted by spinning (16,000 g, 4°C, 10 min). Supernatants were combined (a 20 µL input sample was taken and combined with 20 µL 2 × SDS loading buffer (80 mM Tris-HCl (pH 6.8), 200 mM DTT, 3.2% SDS, 0.1% Bromophenol Blue, 1.6% glycerol)) and added to 0.5 mL of anti-FLAG M2 affinity agarose beads (Sigma) pre-washed with 2 × 10 mL Lysis buffer A (without SUPERase.In). Beads and supernatant were incubated (4°C, 2.5 h) on a nutator, before spinning (1,000 g, 4°C, 2 min). A 20 µL unbound sample was taken and combined with 20 µL 2 × SDS loading buffer. Beads were washed four times with 10 mL Wash buffer A (20 mM HEPES (pH 7.4), 110 mM KOAc, 0.5% Triton X-100, 0.1% Tween 20, 1 mM EDTA). Beads were incubated (30 min, 4°C) twice with 300 µL of Elution buffer (Lysis buffer A with 1 mg/mL 3 × FLAG peptide (Sigma)). The elution supernatants were combined (a 20 µL elute sample was taken and combined with 20 µL 2 × SDS loading buffer) and RNAs were extracted using a miRNeasy kit (QIAGEN) according to the manufacturer's instructions.

Western blotting

Protein samples were separated by gel electrophoresis on 7.5% or 10% SDS polyacrylamide gels and transferred to nitrocellulose membranes. Membranes were incubated with 5% BSA in TBST (20 mM Tris-HCl (pH 7.5), 150 mM NaCl, 0.1% Tween-20) for 2 hr, then primary antibody in 2.5% BSA in TBST for 1.5 hr, washed, then incubated with rabbit, mouse or rat HRP-conjugated secondary antibody

(Sigma) diluted 1:4000 in 2.5% BSA in TBST for 45 min and washed again. Primary antibodies and their dilutions are detailed in the Key Resources Table. Antibody binding was visualized using chemiluminescence (Pierce) and X-ray film.

Library generation

Linker ligation and RNA fragmentation

Immunoprecipitated RNA (3 µg in 30 µL 10 mM Tris-HCl, pH 7.0) was denatured (2 min, 80°C) and placed on ice. A 5′ adenylated, 3′ blocked with a dideoxy C base cloning linker 5rApp/CTGTAGGCACCATCAAT/3ddC (Integrated DNA Technologies) was ligated to the 3′ ends of RNAs by first dividing the RNA into three microfuge tubes and then adding 10 µL ligation reaction mix to give final concentrations of 50 ng μL^{-1} cloning linker 1, 12% PEG 8000, 1 × T4 RNA ligase 2 (Rnl2) (truncated) ligation buffer, 10 U μL^{-1} T4 Rnl2 (truncated) (NEB) and incubating for 3 hr at 37°C. Ligated RNA was incubated (95°C, 35 min) with 20 µL Alkaline fragmentation buffer (100 mM $NaCO_3$ (pH 9.2), 2 mM EDTA) to fragment linker ligated RNA to a narrow size range to reduce size bias of future steps. Fragmentation was not performed for RiboSeq experiments. RNA was precipitated by incubating (30 min, −20°C) with ice cold 500 µL H_20, 60 µL 3 M NaOAc (pH 5.5), 2 µL 15 mg mL^{-1} GlycoBlue (Ambion) and 0.75 mL isopropanol and then spinning (16,000 g, 4°C, 30 min). Pellets were washed with 0.75 mL 80% ethanol, dried (10 min, room temperature) and resuspended sequentially in the same 10 µL 10 mM Tris-HCl (pH 7.0).

Size selection

Ligated and fragmented RNA was mixed with 10 µL 2 × TBE-urea loading dye (89 mM Tris-HCl, 89 mM Boric acid, 2 mM EDTA, 12% Ficoll, 7 M Urea, 2.5 mg/ml Orange G), denatured (2 min, 80°C) and run on a 10 well 10% TBE-urea gel (Biorad) (200 V, 32 min). The gel was stained with SYBRGold (Invitrogen) and the region containing 38-95nt fragments excised. This gel piece was divided between three microfuge tubes and physically disrupted. Each was incubated (70°C, 10 min) in 200 µL H_20. The tubes were pooled and gel debris was removed using a Costar-Spin-X column (Corning). RNA was precipitated by adding 60 µL 3 M NaOAc (pH 5.5), 2 µL 15 mg mL^{-1} GlycoBlue and 0.75 mL isopropanol, incubating (30 min, −20°C) and then spinning (16,000 g, 4°C, 30 min). Pellets were washed with 0.75 mL 80% ethanol, dried (10 min, room temperature) and resuspended in 10 µL 10 mM Tris-HCl (pH 7.0).

Reverse transcription and circularisation

Reverse transcription (RT) was carried out by adding 3.28 µL 5 × FS buffer, 0.82 µL dNTPs (10 mM each), 0.5 µL 100 µM RT primer (This is phosphorylated at the 5′ end (5 Phos) for later circularization and contains two 18 carbon spacer sequences (iSp18)), denaturing (80°C, 2 min) and incubating (48°C, 30 min) with 0.5 µL Superase.In, 0.82 µL 0.1 M DTT, 0.82 µL Superscript III (Invitrogen). 1.8 µL 1 M NaOH was added and RNA was degraded (98°C, 20 min). To neutralize, 1.8 µL 1 M HCl was added. cDNA was mixed with 20 µL 2 × TBE-urea loading dye, denatured (3 min, 95°C), and run (loaded in 2 wells, 20 µL per well) on a 10 well 10% TBE-urea gel (Biorad) (200 V, 50 min). The gel was stained with SYBRGold (Invitrogen) and the regions containing the RT product excised. Both gel pieces were physically disrupted and incubated (70°C, 10 min) in 200 µL H_20 in separate tubes. Gel debris was removed and tubes were pooled. cDNA was precipitated by adding 25 µL 3 M NaCl, 2 µL GlycoBlue and 0.75 mL isopropanol, incubating (−20°C, 30 min) and then spinning (16,000 g, 4°C, 30 min). The

pellet was washed with 0.75 mL 80% ethanol, dried (10 min, room temperature) and resuspended in 15 µL 10 mM Tris-HCl (pH 8.0).

The RT product was circularized by incubating (60°C, 60 min) with 2 µL 10 × CircLigase buffer, 1 µL 1 mM ATP, 1 µL 50 mM $MnCl_2$, 1 µL CircLigase (Epicenter). The enzyme was heat-inactivated at 80°C, 10 min.

PCR amplification

16.7 µL 5 × HF Phusion buffer, 1.7 µL dNTPs (10 mM), 0.4 µL 100 µM Barcoded primer (A, B, C, or D), 0.4 µL 100 µM Primer 1, 59.2 µL H_20, 0.8 µl Phusion polymerase (NEB) was added to 5 µL circularized DNA. This was divided (16.7 µL per tube) between five 0.2 mL tubes. PCR reactions were heated (98°C, 30 s) and then submitted to 7 temperature cycles (98°C, 10 s; 60°C, 10 s; 72°C, 10 s). At the end of cycle 3 and each subsequent cycle one tube was removed and placed on ice. 3.4 µL DNA loading dye (1.5 g Ficoll 400, 25 mg Orange G in 10 mL H_20) was added to each reaction and run on an 8% TBE gel (Invitrogen) (180 V, 55 min). The gel was stained with SYBRGold and the PCR product excised from the PCR reaction with the highest unsaturated signal without higher molecular weight products. The gel piece was physically disrupted and incubated (room temperature, overnight, with agitation) in 0.67 mL DNA soaking buffer (0.3 M NaCl, 10 mM Tris-HCl pH 8.0, 1 mM EDTA). DNA was precipitated by adding 2 µL GlycoBlue and 0.68 mL isopropanol, incubating (−20°C, 30 min) and spinning (16,000 g, 4°C, 30 min). The pellet was washed with 0.75 mL 80% ethanol, dried (10 min, room temperature) and resuspended in 10 µL 10 mM Tris-HCl (pH 8.0).

Sequencing

Samples were submitted to Harvard Biopolymers facility. They determined DNA quality and quantity using the TapeStation (Agilent) and qPCR and then sequenced samples on an Illumina HiSeq 2000 machine or a NextSeq500 machine. 50nt were sequenced from one end using the sequencing primer. Barcoded samples were pooled so that 2-3 samples were multiplexed per lane.

Polysome fractionation.

Samples were resuspended in 400 ul of polysome lysis buffer (20 mM HEPES pH 8.0, 50 mM KCl, 10 mM $MgCl_2$, 1% Triton-X100, 100 ug/ml cycloheximide, 1 mM DTT, cOmplete EDTA-free protease inhibitors – Roche) plus 500 ul acid-washed glass beads (Sigma-Aldrich) and subjected to 8 cycles of lysis in a MagNALyser (Roche – 6000 rpm, 1 min on, 2 min off). Lysate was transferred to fresh microfuge tubes and clarified by centrifugation (13,000 rpm, 10 min, 4 °C).

Lysate containing 2 mg of protein was loaded onto the top of a 7-47 % sucrose gradient in polysome gradient buffer (20 mM HEPES pH 8.0, 50 mM KCl, 10 mM $MgCl_2$, 100 ug/ml cycloheximide) and macromolecular complexes were separated by velocity gradient ultracentrifugation (SW41Ti – Beckman, 39,000 rpm, 2 hr, 4°C). Fractions were collected using Biocomp Gradient Station and pooled to obtain separate monosomal and polysomal fractions. RNA was extracted from pooled fractions and input samples (miRNeasy – Qiagen) for 3'-end sequencing (QuantSeq for Ion Torrent – Lexogen). Fixed quantities of *S. pombe* RNA were added prior to RNA extraction for the purposes of internal calibration (polysomal - 1 $ug_{pombe\ RNA}/mg_{lysate}$, monosomal - 1 $ug_{pombe\ RNA}/mg_{lysate}$, input – 30 $ug_{pombe\ RNA}/mg_{lysate}$). No polysomal libraries were generated in this study.

3'-end Sequencing of Total mRNA.

1 ml of cycling *CENPK113-7D rpb3-FLAG* in YMC-YE media (OD_{600} approx. 16.9) was combined with 2.8 OD_{600} of *S. pombe* and total RNA was isolated by hot acid-phenol extraction. 500 ng of total RNA was used to generate 3'end Seq libraries using the QuantSeq for Ion Torrent kit (Lexogen) and libraries were sequenced on the Ion Proton platform.

Extraction of Total Protein.

1 ml of cycling *CENPK113-7D rpb3-FLAG* in YMC-YE media (OD_{600} approx. 16.9) was centrifuged (7,000 rpm, 1 min), the supernatant was removed and the pellet was flash-frozen in $N_{2(l)}$. Pellets were thawed, washed twice in 1x PBS (5000 rpm, 3 min, 4°C) and resuspended in proteome lysis buffer (50 mM Tris HCl pH 8.0, 8 M urea, 75 mM NaCl, 100 mM sodium butyrate, cOmplete protease inhibitors – Roche). Cells were then mechanically lysed (MagNAlyzer Roche – 6000 rpm, 1 min on, 2 min off) in the presence of 300 ul acid-washed glass beads (Sigma-Aldrich).

Unlabelled Proteome.

Protein samples were digested according to the FASP procedure described in Wisniewski *et al*. 2009. After digestion, peptides were separated by nano-flow reversed-phase liquid chromatography coupled to Q Exactive Hybrid Quadrupole-Orbitrap mass spectrometer (Thermo Fisher Scientific) using HCD fragmentation. In brief, peptides were loaded on a C18 PepMap100 pre-column (300 µm i.d. x 5 mm, 100Å, Thermo Fisher Scientific) at a flow rate of 12 µL/min in 100% buffer A (0.1% FA in water). Peptides were then transferred to a 50cm in-house packed analytical column heated at 45°C (75 µm i.d. packed with ReproSil-Pur 120 C18-AQ, 1.9 µm, 120 Å, Dr.Maisch GmbH) and separated using a 60 min gradient from 15 to 35% buffer B (0.1% FA in ACN) at a flow rate of 200 nL/min. Q Exactive survey scans were acquired at 70,000 resolution to a scan range from 350 to 1500 m/z, AGC target 3e6, maximum injection time 50 ms. The mass spectrometer was operated in a data-dependent mode to automatically switch between MS and MS/MS. The 10 most intense precursor ions were submitted to HCD fragmentation using an MS/MS resolution set to 17 500, a precursor AGC target set to 5e4, a precursor isolation width set to 1.5 Da, and a maximum injection time set to 120 ms. MS/MS spectra were searched against the relevant Uniprot proteome database using MaxQuant, version 1.5.0.35 (Tyanova *et al.* 2016); precursor mass tolerance was set to 20 ppm and MS/MS tolerance to 0.05 Da. Enzyme specificity was set to trypsin with a maximum of two missed cleavages. False discovery rate for protein and peptide spectral matches was set at 0.01.

Western Blotting.

1 ml samples from a cycling culture were centrifuged (7000 rpm, 15s), the supernatant was removed and the pellets were flash-frozen in $N_{2(l)}$. Pellets were thawed, resuspended in 600 ul loading buffer (50 mM Tris.HCl pH 8.0, 4 M urea, 100 mM DTT, 10 % glycerol, 2 % SDS, 0.05 % bromophenol blue) and mechanically homogenized using acid-washed glass beads for 3 min (Sigma-Aldrich) then incubated at 95 °C for 5 min. Proteins were resolved by SDS-PAGE and transferred to PVDF membranes by wet-transfer blotting (25 V, 16 hr, 4 °C). Membranes were blocked for 1 hour in TBST + 5 % BSA, before being treated with primary antibodies in TBST + 2.5 % BSA under the indicated conditions then 3x washed with TSBT. Secondary antibody treatments were performed for 45 min at a dilution of 1:2000 in TBST + 2.5 % BSA at 25 °C and follwed with 3x washes in TBST. Proteins were detected by electrochemiluminesence which was recorded either using x-ray film or using an iBright western blot imager (ThermoFisherScientific).

Quantification and Statistical Analysis

Aligning NGS data

RiboSeq data was aligned using Tophat (citation) to a combined *S. cerevisiae/S. pombe* genome using the following parameters: -N 1 -l 2000 -g 5 --b2-N 1 --b2-L 28 -G (gtf file) –no-novel-juncs, and uniquely aligned reads were extracted using samtools view -bq 49. Files were converted to .bed and .bedgraph format using bedtools for further analysis.

NET-Seq data was aligned using bowtie (citation) using the following parameters: -q -p 16 -S -m 1 -n 1 -e 70 -l 28 -k 1 --best –phred33-quals, converted to a .bam file using samtools view -Sb, then into .bed and .bedgraph files using bedtools (citation).

3'-end Seq data was aligned to a combined *S. cerevisiae/S. pombe* genome using STAR (citation) with the following parameters: --runThreadN 8 --genomeDir [STARfiles] --readFilesIn [input_file] --outFilterType BySJout --outFilterMultimapNmax 20 --alignSJoverhangMin 8 --alignSJDBoverhangMin 1 --outFilterMismatchNmax 999 outsFilterMismatchNoverLmax 0.08 --alignIntronMin 13 --alignIntronMax 2482 --outFileNamePrefix [output_file]. Uniquely aligned reads were extracted using samtools view -Sbq 20 and converted to .bed format using bedtools bamtobed for further analysis. Raw counts tables were generated from .bed files in R using the summarizeoverlaps function.

Library Size Calibration

For 3'-end Seq data from total RNA, library sizes were calibrated to *S. pombe* counts as an internal control, using the estimateSizeFactorsforMatrix command from DESeq2. 3'-end Seq from gradient-fractionated RNA was normalized in the same way, but to the *S. cerevisiae* library sizes (i.e. without internal calibration).

For NET-Seq data, library sizes were calibrated to *S. pombe* counts as an internal control by multiplying by the following normalization factor [(mass of *S. pombe* paste)/(total *S. pombe* reads * mass of *S. cerevisiae* paste)].

For RiboSeq data, library sizes were calibrated to *S. pombe* counts as an internal control.

Cluster Analysis

To cluster genes based on their temporal profiles at the transcription, transcript or protein level respectively, calibrated counts for each gene were transformed to obtain log2 fold-change in expression over time versus the median. Transformed data was then partitioned using k-means++ clustering into the optimal number of clusters, as determined by the Gap-Statistic and silhouette methodologies.

Metrics for Dispersion and Oscillation

The coefficient of variation (mean/standard deviation) of signal over time was used to quantify the relative amplitude of cycling variation in potentially cycling 3'-end Seq and proteomics datasets. Signals that oscillate with a large amplitude will have a larger standard deviation over time whereas their mean signal should be invariate. To determine whether variation in signal was continuous or stochastic over time, the autocorrelation at offset +1 was calculated.

Western Blot Quantification

Band intensity for Western blotting experiments was quantified using ImageJ and data was analysed in R using ANOVA and Tukey's honest significant difference test. A p-value of less than 0.05 was considered statistically significant.

Data and Code Availability

All sequencing data generated in this study is available at:

https://www.ncbi.nlm.nih.gov/geo/query/acc.cgi?acc=GSE138023.

KEY RESOURCES TABLE

REAGENT or RESOURCE	SOURCE	IDENTIFIER
Antibodies		
Mouse anti-puromycin	Sigma-Aldrich	Cat# MABE343, RRID:AB_2566826
Mouse anti-actin	Abcam	Cat# ab14128, RRID:AB_300931
Mouse anti-myc	Sigma-Aldrich	Cat# M5546, RRID:AB_260581
Rat anti-tubulin	Abcam	Cat# ab6160, RRID:AB_305328
Rabbit anti-Rps6	Abcam	Cat# ab40820, RRID:AB_945319
Rabbit Anti Rps6 phospho S235/236	Abcam	Cat# ab12864, RRID:AB_299486
Rabbit Anti-Histone H3	MIllipore	Cat# 05-928, RRID:AB_492621
Mouse Anti-FLAG	Sigma-Aldrich	Cat# F3165, RRID:AB_259529
Chemicals, Peptides, and Recombinant Proteins		
Phos-Tag Acrylamide	FUJIFILM Wako Pure Chemical Corporation	300-93523 (AAL-107M)
RNaseI	Ambion	AM2294
FLAG peptide	Sigma-Aldrich	F4799
T4 RNA ligase II (Truncated)	NEB	M0242L
PNK	NEB	M0201S
Circligase	Cambio	CL4115K
Critical Commercial Assays		
QuantSeq 3' mRNA-Seq Library Prep Kit for Ion Torrent (A)	Lexogen	012.24A.
QuantSeq 3' mRNA-Seq Library Prep Kit for Ion Torrent (B)	Lexogen	012.24B.
miRNEasy mini-kit	Qiagen	217004
Deposited Data		
Raw and Analyzed Data	This Study	GEO **GSE133934**
Histone acetylation YMC ChIP-Seq (ln fold-change)	S. Casani	
Protein stability dataset	Lahtvee et al., 2017	

Experimental Models: Organisms/Strains

Saccharomyces cerevisiae CENPK113-7D rpb3-FLAG::KANMX6This Study

Saccharomyces cerevisiae CENPK113-7D Gift from Boeke Lab CENPK113-7D

Schizosaccharomyces pombe Gift from Vasilijeva Lab

Oligonucleotides

Linker-1:5'-AppCTGTAGGCACCATCAAT/3ddC-3' This Study

RT-primer:
5'/5Phos/ATCTCGTATGCCGTCTTCTGCTTG/iSp18/CACTCA/iSp18/TCCGACGATCATTGATGGTG CCTACAG 3'

(iSp18 is carbon spacer) – (5 ' is phosphorylated) This Study

ONTI230: 5'

CAAGCAGAAGACGGCATACGA

3'

Barcoding primer 1

NS(oLSC008-bc1): 5'
AATGATACGGCGACCACCGAGATCTACACGATCGGAAGAGCACACGTCTGAACTCCAGTCACAT GCCATCCGACGATCATTGATGG 3'

Barcoding primer 2

NS(oLSC008-bc2): 5'
AATGATACGGCGACCACCGAGATCTACACGATCGGAAGAGCACACGTCTGAACTCCAGTCACTG CATCTCCGACGATCATTGATGG 3'

Barcoding primer 4

NS(oLSC008-bc4): 5'
AATGATACGGCGACCACCGAGATCTACACGATCGGAAGAGCACACGTCTGAACTCCAGTCACTT AGGCTCCGACGATCATTGATGG 3'

Barcoding primer 5

NS(oLSC008-bc5): 5'
AATGATACGGCGACCACCGAGATCTACACGATCGGAAGAGCACACGTCTGAACTCCAGTCACTG ACCATCCGACGATCATTGATGG 3'

Software and Algorithms

Samtools Li et al., 2009 http://samtools.sourceforge.net/

Bedtools Quinlan & Hall, 2010 https://bedtools.readthedocs.io/en/latest/#

Bowtie2Langmead and Salzberg, 2012 http://bowtie-bio.sourceforge.net/bowtie2/index.shtml

R The R-Project https://www.r-project.org/about.html

STAR Dobin et al., 2012 http://code.google.com/p/rna-star/.

Figure Legends

Figure 1

The cycling transcriptome of the YMC is primarily driven by transcriptional oscillations.

11 NETSeq and 22 polyA-primed RNASeq samples were taken from *CENPK113-7D rpb3-FLAG::KANMX6* cells cycling at a dilution rate of 0.082 hr^{-1}. Counts tables were generated from both datasets for all *S. cerevisiae* genes and for each gene and dataset, a log2 fold-change vs median transformation was applied. Gap-Statistic analysis was applied to the transformed NETSeq data to determine the correct number of clusters into which to divide genes using the k-means++ algorithm (A). For both datasets, the transformed data was divided into three clusters using the k-means++ algorithm and the overlap of the cluster:cluster overlap was plotted as a heatmap (B). Transformed NETSeq and RNASeq data was divided into the same three NETSeq clusters and plotted over time alongside all genes. Mean profiles were also plotted for each dataset and cluster (C). The NETSeq counts tables were normalized to gene-length, then log2(x+1) transformed and plotted over time. Profiles were colour-coded based on cluster membership (red – HOC-T; blue – LOC-T, tan – TI-T). Mean profiles for each cluster were also plotted (D). log2(x+1) transformed data was divided into the NETSeq clusters then divided into octiles based on median expression level. Mean expression over time was plotted for each octile (E).

Figure 2

The proteome of the Yeast Metabolic Cycle is static.

Two proteomes were generated using TMT-labelled (10 samples) and unlabelled mass-spectrometry (6 samples) from soluble protein extracts from the yeast metabolic cycle. A Venn diagram was generated to show the overlap of proteins with coverage over all timepoints between datasets (A) and the distributions of the three RNASeq clusters in the TMT-labelled dataset and in both datasets were plotted as pie charts (B). A log2 fold-change vs median transformation was applied to the RNASeq data and the TMT-labelled proteomics and both were divided into the RNASeq clusters and plotted over time (C). For each gene, the coefficient of variation of log2 fold-change vs median transformed data was calculated for the RNASeq dataset and both proteomes. These values were used to generate box plots splitting the data by dataset and RNASeq cluster. The statistical significance of the difference between the means of TI-R genes and HOC or LOC genes was calculated for each dataset using Dunnett's Test. Raw p-values are displayed (D). The autocorrelation of log2 fold-change vs median transformed data was calculated for each gene for the RNASeq dataset and both proteomes. These values were used to generate box plots splitting the data by dataset and RNASeq cluster. The statistical significance of the difference between the means of TI-R genes and HOC or LOC genes was calculated for each dataset using Dunnett's Test. Raw p-values are displayed (E).

Figure 3

Buffering of the YMC proteome to cycling transcript levels occurs as a result of low protein turnover.

Three models for how the proteome may be buffered against transcriptional changes. (Topmost) Translation rates are constant. Despite the transcriptome cycling, protein synthesis rates for individual genes are constitutive, meaning that protein levels too are constant. (Central) Perfect coordination of

synthesis and degradation. Cycling transcripts lead to cycling protein synthesis rates. However, protein degradation rates also cycle which cancels out any changes in levels. (Bottom) Slow protein turnover minimizes the impact of cycling transcripts. Cycling of transcripts leads to cycling of protein synthesis rates. However, only a minimal amount of protein is synthesized and degraded each cycle, meaning that the amplitude of cycling protein levels is negligible.

Figure 4

Post-transcriptional modifications to Rps6 and histones and ribosome assembly vary throughout the YMC.

(A) Levels of Rps6 protein do not cycle in the YMC consistent with the proteomic data. The doubly phosphorylated form of Rps6 also phosphorylates. Representative western blots are shown and quantitation of n=3 experimental repeats. (B) Levels of rRNA during the YMC determined by RNA FISH to spacer regions allowing assessment of rates of transcription before processing. Levels of rRNA production peak in the HOC phase of the cycle. Levels of substantially lower than in exponentially growing cultures. Images show that most cells express rRNA at the peak. This suggests that ribosome assembly is coordinated during the YMC. (C) Variations in levels of transcription (NET-seq), Rsc2 (by ChIP)) and H3K14ac (by ChIP) over genes during the YMC. The data is clustered into the groups shown in Figure 1. Rsc2 and H3K14ac is enriched alternatively on the HOC genes and LOC genes suggesting competition between these groups for expression. The third group are not enriched for H3K14ac or Rsc2 and do not show cycling transcription.

Supplementary data figure 1. (A). Alternative phases of high and low oxygen consumption in the YMC assessed in the synchronised culture using an O_2 electrode. These profiles allow sampling to be coordinated between experiments as the cycle length is highly reproducible. (B) FACS analysis of strains stained with propidium iodine revealing the DNA content and the period of S phase. About 10% of cells enter S phase during the cycle. (c). Statistics for clustering RNA-seq and NET-seq data to support Figure 1.

Figure 1

(Central) Perfect coordination of synthesis and degradation

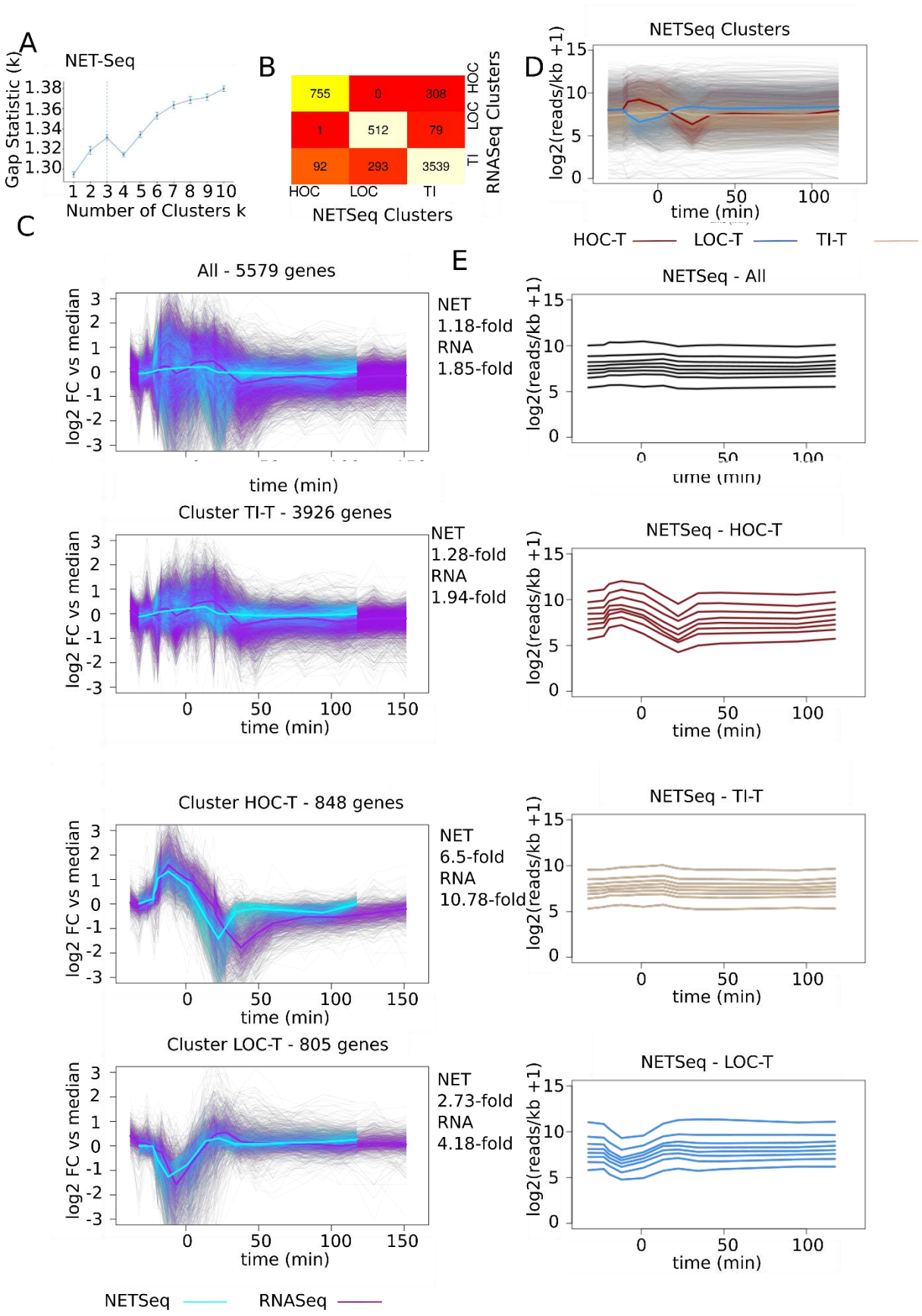

Figure 2

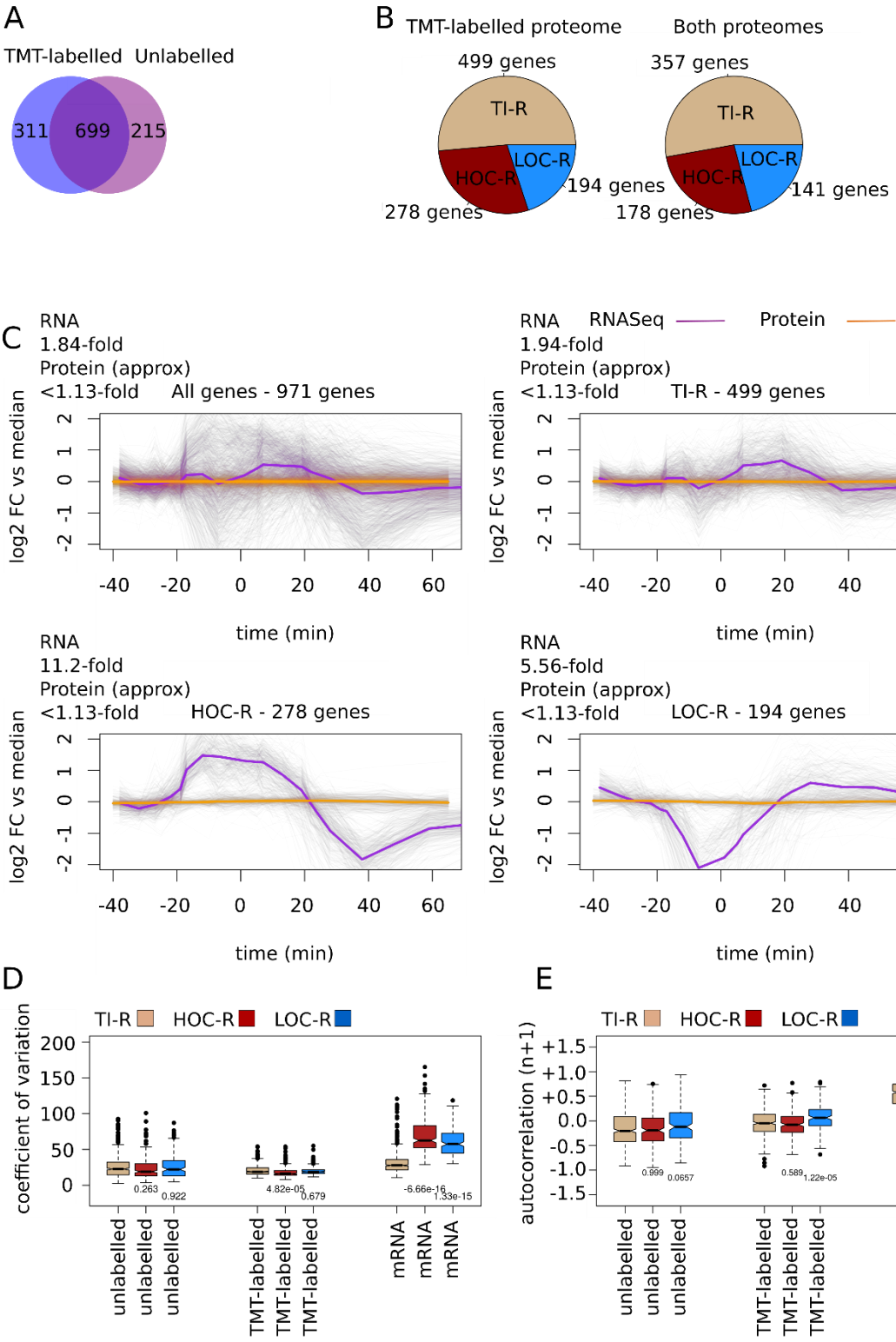

Figure 3

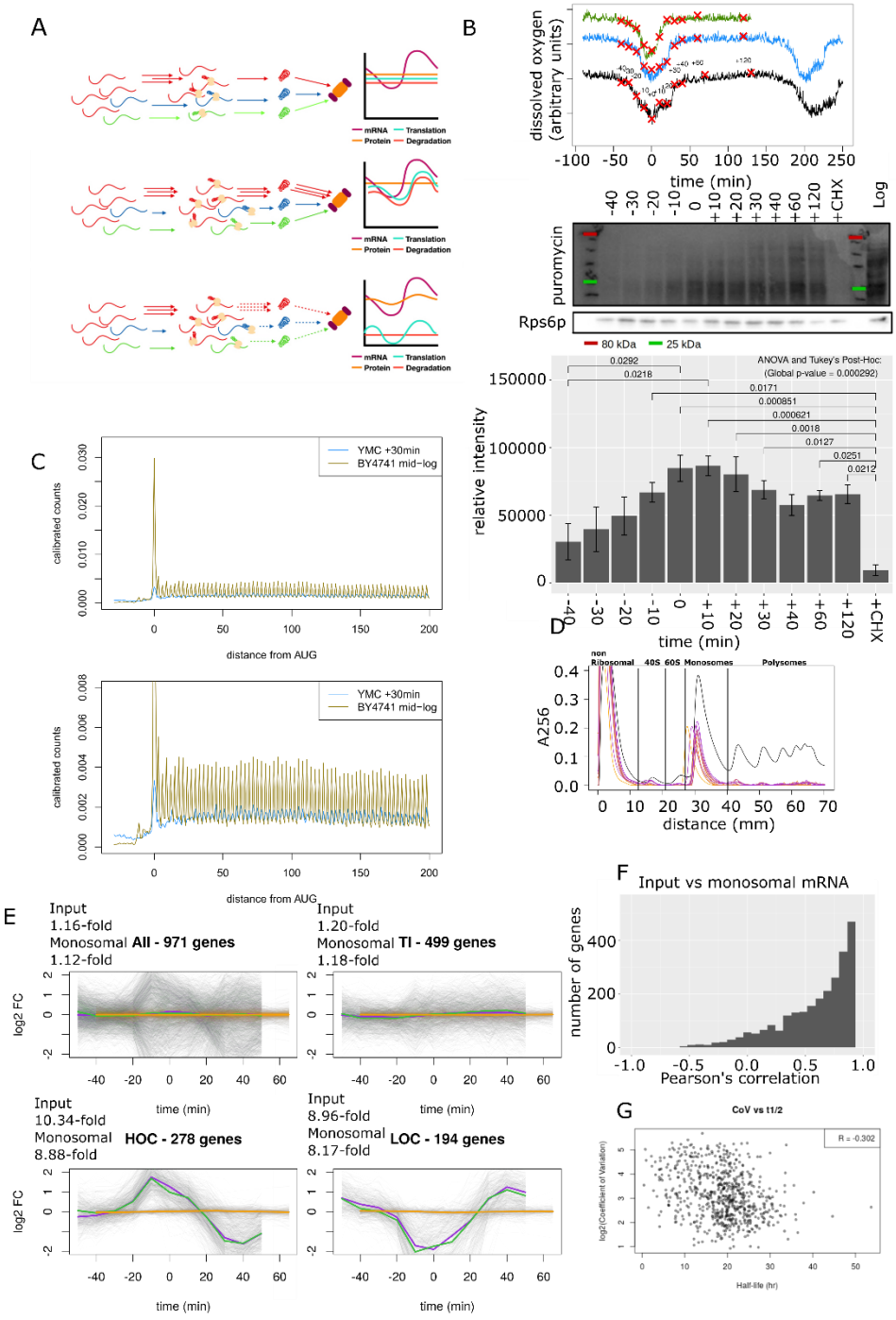

Figure 4

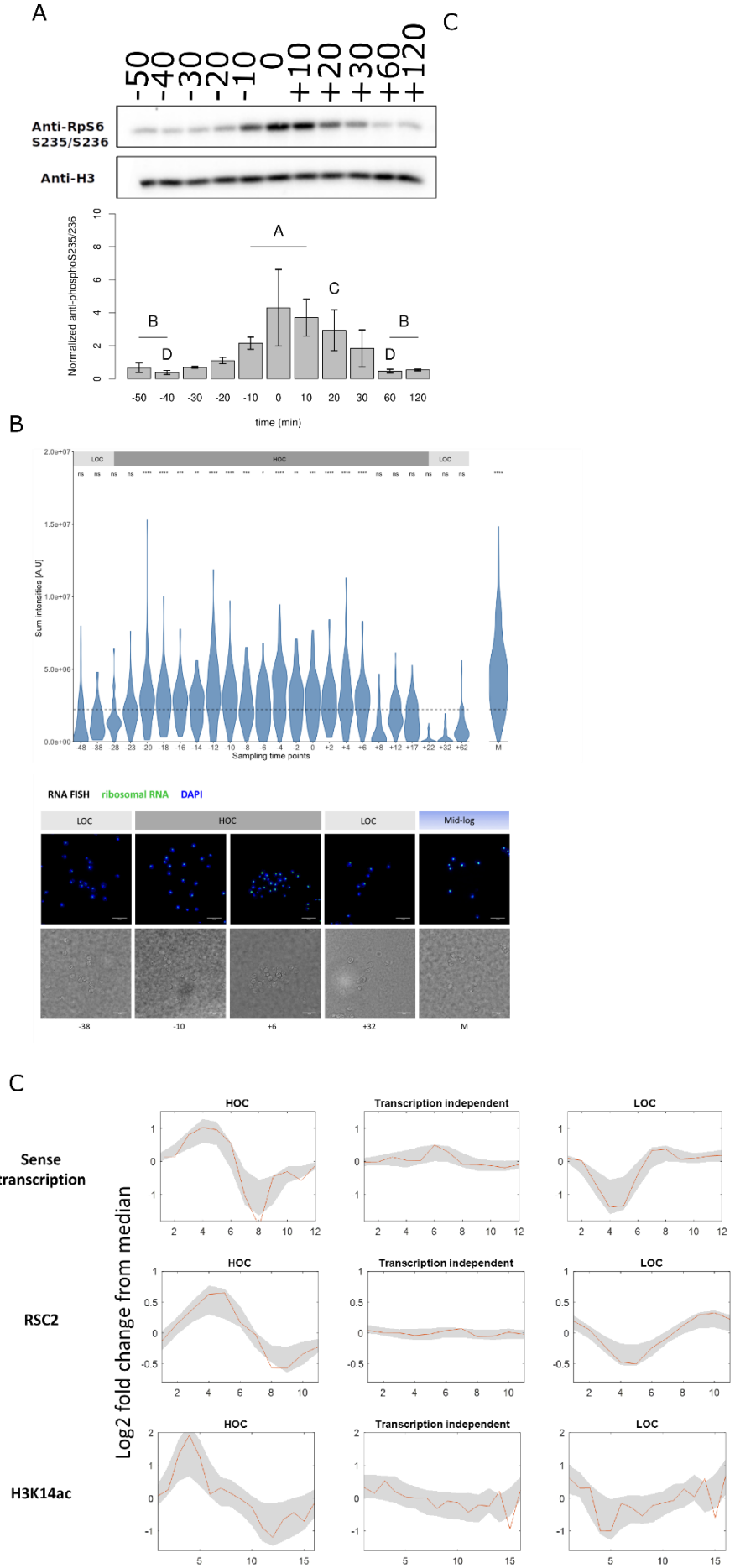

Figure S1

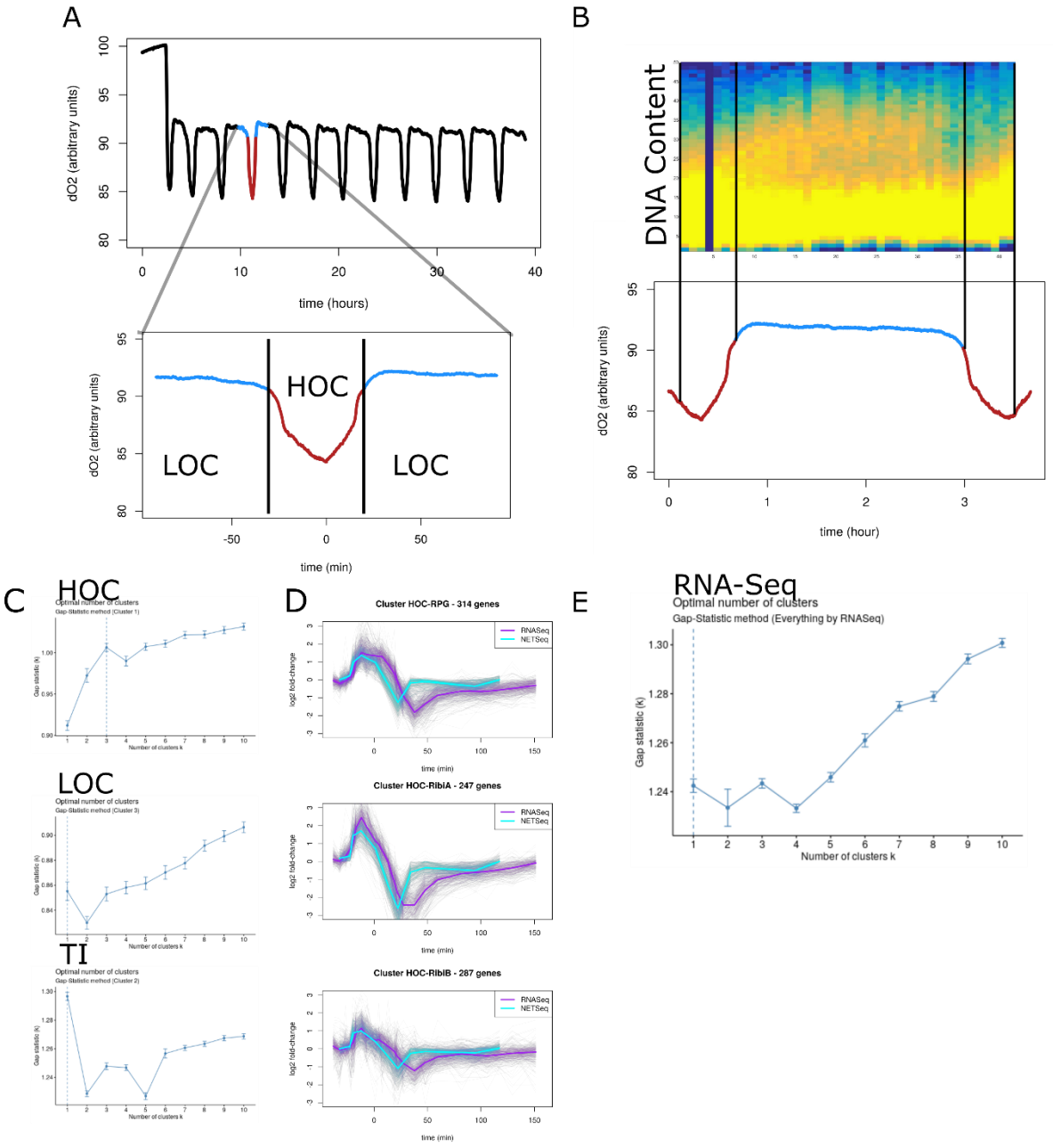

Ahuatzi, D., Riera, A., Pelaez, R., Herrero, P., and Moreno, F. (2007). Hxk2 regulates the phosphorylation state of Mig1 and therefore its nucleocytoplasmic distribution. J Biol Chem *282*, 4485-4493.

Banerji, S.S., Theodorakis, N.G., and Morimoto, R.I. (1984). Heat shock-induced translational control of HSP70 and globin synthesis in chicken reticulocytes. Mol Cell Biol *4*, 2437-2448.

Cai, L., and Tu, B.P. (2011). Acetyl-CoA drives the transcriptional growth program in yeast. Cell Cycle *10*, 3045-3046.

Cairns, B.R., Lorch, Y., Li, Y., Zhang, M., Lacomis, L., Erdjument-Bromage, H., Tempst, P., Du, J., Laurent, B., and Kornberg, R.D. (1996). RSC, an essential, abundant chromatin-remodeling complex. Cell *87*, 1249-1260.

Caster, S.Z., Castillo, K., Sachs, M.S., and Bell-Pedersen, D. (2016). Circadian clock regulation of mRNA translation through eukaryotic elongation factor eEF-2. Proc Natl Acad Sci U S A *113*, 9605-9610.

Causton, H.C., Feeney, K.A., Ziegler, C.A., and O'Neill, J.S. (2015). Metabolic Cycles in Yeast Share Features Conserved among Circadian Rhythms. Curr Biol *25*, 1056-1062.

Churchman, L.S., and Weissman, J.S. (2011). Nascent transcript sequencing visualizes transcription at nucleotide resolution. Nature *469*, 368-373.

Fischl, H., Howe, F.S., Furger, A., and Mellor, J. (2017). Paf1 Has Distinct Roles in Transcription Elongation and Differential Transcript Fate. Mol Cell *65*, 685-698 e688.

Gonzalez, A.M., Hoffman, J.R., Jajtner, A.R., Townsend, J.R., Boone, C.H., Beyer, K.S., Baker, K.M., Wells, A.J., Church, D.D., Mangine, G.T.*, et al.* (2015). Protein supplementation does not alter intramuscular anabolic signaling or endocrine response after resistance exercise in trained men. Nutr Res *35*, 990-1000.

Herrero, P., Martinez-Campa, C., and Moreno, F. (1998). The hexokinase 2 protein participates in regulatory DNA-protein complexes necessary for glucose repression of the SUC2 gene in Saccharomyces cerevisiae. FEBS Lett *434*, 71-76.

Ingolia, N.T., Ghaemmaghami, S., Newman, J.R., and Weissman, J.S. (2009). Genome-wide analysis in vivo of translation with nucleotide resolution using ribosome profiling. Science *324*, 218-223.

Jambunathan, N., Martinez, A.W., Robert, E.C., Agochukwu, N.B., Ibos, M.E., Dugas, S.L., and Donze, D. (2005). Multiple bromodomain genes are involved in restricting the spread of heterochromatic silencing at the Saccharomyces cerevisiae HMR-tRNA boundary. Genetics *171*, 913-922.

Klevecz, R.R., Bolen, J., Forrest, G., and Murray, D.B. (2004). A genomewide oscillation in transcription gates DNA replication and cell cycle. Proc Natl Acad Sci U S A *101*, 1200-1205.

Kouzarides, T. (2007). Chromatin modifications and their function. Cell *128*, 693-705.

Kuang, Z., Cai, L., Zhang, X., Ji, H., Tu, B.P., and Boeke, J.D. (2014). High-temporal-resolution view of transcription and chromatin states across distinct metabolic states in budding yeast. Nat Struct Mol Biol *21*, 854-863.

Lahtvee, P.J., Sanchez, B.J., Smialowska, A., Kasvandik, S., Elsemman, I.E., Gatto, F., and Nielsen, J. (2017). Absolute Quantification of Protein and mRNA Abundances Demonstrate Variability in Gene-Specific Translation Efficiency in Yeast. Cell Syst *4*, 495-504 e495.

Lee, C.D., and Tu, B.P. (2015). Glucose-Regulated Phosphorylation of the PUF Protein Puf3 Regulates the Translational Fate of Its Bound mRNAs and Association with RNA Granules. Cell Rep *11*, 1638-1650.

Liu, Y., Beyer, A., and Aebersold, R. (2016). On the Dependency of Cellular Protein Levels on mRNA Abundance. Cell *165*, 535-550.

Mellor, J. (2016). The molecular basis of metabolic cycles and their relationship to circadian rhythms. Nat Struct Mol Biol *23*, 1035-1044.

Noya, S.B., Colameo, D., Bruning, F., Spinnler, A., Mircsof, D., Opitz, L., Mann, M., Tyagarajan, S.K., Robles, M.S., and Brown, S.A. (2019). The forebrain synaptic transcriptome is organized by clocks but its proteome is driven by sleep. Science *366*.

Ray, S., and Reddy, A.B. (2016). Cross-talk between circadian clocks, sleep-wake cycles, and metabolic networks: Dispelling the darkness. Bioessays *38*, 394-405.

Sanchez-Gaya, V., Casani-Galdon, S., Ugidos, M., Kuang, Z., Mellor, J., Conesa, A., and Tarazona, S. (2018). Elucidating the Role of Chromatin State and Transcription Factors on the Regulation of the Yeast Metabolic Cycle: A Multi-Omic Integrative Approach. Frontiers in genetics *9*, 578.

Skalska, L., Beltran-Nebot, M., Ule, J., and Jenner, R.G. (2017). Regulatory feedback from nascent RNA to chromatin and transcription. Nat Rev Mol Cell Biol *18*, 331-337.

Storti, R.V., Scott, M.P., Rich, A., and Pardue, M.L. (1980). Translational control of protein synthesis in response to heat shock in D. melanogaster cells. Cell *22*, 825-834.

Tissieres, A., Mitchell, H.K., and Tracy, U.M. (1974). Protein synthesis in salivary glands of Drosophila melanogaster: relation to chromosome puffs. J Mol Biol *84*, 389-398.

Tsang, C.K., Liu, H., and Zheng, X.F. (2010). mTOR binds to the promoters of RNA polymerase I- and III-transcribed genes. Cell Cycle *9*, 953-957.

Tu, B.P., Kudlicki, A., Rowicka, M., and McKnight, S.L. (2005). Logic of the yeast metabolic cycle: temporal compartmentalization of cellular processes. Science *310*, 1152-1158.

Tu, B.P., and McKnight, S.L. (2006). Metabolic cycles as an underlying basis of biological oscillations. Nat Rev Mol Cell Biol *7*, 696-701.

Vega, M., Riera, A., Fernandez-Cid, A., Herrero, P., and Moreno, F. (2016). Hexokinase 2 Is an Intracellular Glucose Sensor of Yeast Cells That Maintains the Structure and Activity of Mig1 Protein Repressor Complex. J Biol Chem *291*, 7267-7285.

Yerlikaya, S., Meusburger, M., Kumari, R., Huber, A., Anrather, D., Costanzo, M., Boone, C., Ammerer, G., Baranov, P.V., and Loewith, R. (2016). TORC1 and TORC2 work together to regulate ribosomal protein S6 phosphorylation in Saccharomyces cerevisiae. Mol Biol Cell *27*, 397-409.